

# ${}^7\text{Li}(p,n)$ NUCLEAR DATA LIBRARY FOR INCIDENT PROTON ENERGIES TO 150 MEV

S. G. Mashnik, M. B. Chadwick, H. G. Hughes, R. C. Little, R. E. MacFarlane,  
L. S. Waters, and P. G. Young  
*Los Alamos National Laboratory, Los Alamos, NM 87545, USA*

February 8, 2008

## ABSTRACT

Researchers at Los Alamos National Laboratory are considering the possibility of using the Low Energy Demonstration Accelerator, constructed at Los Alamos Neutron Science Center for the Accelerator Production of Tritium Project, as a neutron source. Evaluated nuclear data are needed for the  $p+{}^7\text{Li}$  reaction, to predict neutron production from thin and thick lithium targets. In this paper we describe evaluation methods that make use of experimental data, and nuclear model calculations, to develop an ENDF-formatted data library for incident protons with energies up to 150 MeV. The important  ${}^7\text{Li}(p,n_0)$  and  ${}^7\text{Li}(p,n_1)$  reactions are evaluated from the experimental data, with their angular distributions represented using Legendre polynomial expansions. The decay of the remaining reaction flux is estimated from GNASH nuclear model calculations. This leads to the emission of lower-energy neutrons and other charged particles and gamma-rays from preequilibrium and compound nucleus decay processes.

The evaluated ENDF-data are described in detail, and illustrated in numerous figures. We also illustrate the use of these data in a representative application by a radiation transport simulation with the code MCNPX.

## I. INTRODUCTION

As a part of the Accelerator Production of Tritium (APT) Project [1], the Low Energy Demonstration Accelerator (LEDA) has been constructed at the Los Alamos Neutron Science Center (LANSCE) [2]. LEDA is a high-current low-energy proton accelerator that can be used to provide a source of neutrons, following proton bombardment on suitable targets. For instance, high-Z targets can be used to produce spallation neutrons. However, there is a recent interest in the use of a  ${}^7\text{Li}$  target, which, when bombarded with protons, can produce a relatively high yield of quasimonoenergetic neutrons in the forward direction via the  ${}^7\text{Li}(p,n)$  reaction. In particular, this reaction may be useful to provide neutrons with energies near 14 MeV, for materials testing for the fusion program.

In addition to the above application, quasimonoen-

ergetic and broad neutron sources are needed for research in other areas in nuclear science and technology, *e.g.* Accelerator Transmutation of Waste (ATW), radiation damage studies, medical isotope production, and physics cross section experiments.

In order to assess the feasibility of using a lithium target to produce neutrons, accurate evaluated cross section data are needed. These data can be used to predict the neutron yield, as well as the neutron energy and angular dependencies, from both thin and thick targets. (Thin targets allow the possibility of producing quasimonoenergetic neutron sources<sup>1</sup>, whereas thicker targets produce broad-spectrum neutron sources.)

Table-based charged-particle transport is a new feature of the MCNPX transport code system and has been implemented for protons in the developmental version [3]. Proton evaluations for energies up to 150 MeV have been completed about a year ago for 42 isotopes [4]. The present study extends our library for  ${}^7\text{Li}$ , not covered by [4]. A detailed report on our work may be found in [5].

## II. AN OVERVIEW OF AVAILABLE ${}^7\text{Li}(p,xn)$ DATA

An overview of reactions used for the production of fast quasimonoenergetic neutrons, including the  ${}^7\text{Li}(p,xn)$  reaction, may be found in our report [5] and in the comprehensive review by Drogg [6]. Natural lithium consists of isotopes  ${}^6\text{Li}$  and  ${}^7\text{Li}$  with abundances 7.42 and 92.58%, respectively. The  ${}^7\text{Li}(p,n){}^7\text{Be}$  reaction was reviewed in 1960 by Gibbons and Newson [7]. Useful information on kinematics and technical aspects related to the use of  ${}^{nat}\text{Li}$  may be found in [8].

Experimentally, the  ${}^7\text{Li}(p,n)$  reaction was measured by several groups:

A) From threshold to about 8 MeV, by Meadows and Smith, using the Argonne Fast-Neutron Generator [9, 10];

B) From 10 to about 20 MeV, by Anderson *et al.*, at

---

<sup>1</sup>Though our results shown in this paper indicate that once the incident proton energy exceeds a few-MeV, even thin targets result in a substantial number of lower-energy neutrons.

Lawrence Radiation Laboratory [11], and from 4.3 to 26 MeV, by Poppe *et al.* using EN tandem Van de Graaff accelerator (and AVF cyclotron, for  $E_p > 15$  MeV) at Livermore [12]. Poppe *et al.* have been summarized in Ref. [12] practically all measurements of this reaction before 1976;

C) At 15, 20, and 30 MeV, by McNaughton *et al.*, at the Croker Nuclear Laboratory [13];

D) By a number of other groups (see, e.g., [14-18]), at proton energies above 20 MeV.

Between 1.9 and 2.4 MeV bombarding energy, the neutrons are monoenergetic and the reaction cross section is large. Therefore the  ${}^7\text{Li}(p,n){}^7\text{Be}$  reaction has long been used as a source of neutrons ( $n_0$ ) at these energies [7].

Above 2.4 MeV the first excited state of  ${}^7\text{Be}$  at 0.43 MeV may be excited, producing a second group of neutrons ( $n_1$ ). However, below 5 MeV the zero-degree yield of these low energy neutrons is less than about 10% of the ground-state yield, so that the usefulness of the reaction as a monoenergetic neutron source is only slightly impaired.

Above 3.68 MeV, the threshold for the three-body breakup reaction  ${}^7\text{Li}(p,n){}^3\text{He}{}^4\text{He}$ , neutrons from this mode contribute also to the total neutron yield. The zero-degree neutron spectra from this mode are very broad, of an evaporative-type form, and were measured up to  $E_p = 7.7$  MeV by Meadows and Smith [10].

Above 7.06 MeV, the threshold for the reaction  ${}^7\text{Li}(p,n){}^7\text{Be}$  with excitation of the second excited state of  ${}^7\text{Be}$ , neutrons from this mode ( $n_2$ ) also begin to contribute to the total neutron yield, but this contribution is not significant [10]. Therefore, the usefulness of the  ${}^7\text{Li}(p,n){}^7\text{Be}$  reaction as a source of neutrons at energies above 5-7 MeV would depend on a particular application. Only a very good energy resolution would allow one to separate the substantial number of  $n_1$  neutrons to obtain a monoenergetic source. However, if the application can tolerate including both  $n_0$  and  $n_1$  neutron groups, then the reaction has the favorable feature of use of a cheap solid target with a forward angle laboratory cross section approaching 7.4 mb/sr at  $E_p = 15$  MeV and 14.5 mb/sr at  $E_p = 20$  MeV. It should be noted that although the neutron yield is large, the presence of low energy neutrons from different reaction modes may limit the usefulness of the  ${}^7\text{Li}(p,n){}^7\text{Be}$  reaction as a monoenergetic neutron source at proton energies above 10 MeV [12].

The  $n_0$  and  $n_1$  neutron yields are strongly forward peaked. Their measured cross section increases monotonically with increasing  $E_p$  (see Table II in [5]). This is not true for the total neutron cross sections integrated over all emission angles, shown for  $E_p < 26$  MeV in Fig. 1 (see [5] for a compilation of all available data).

One can see that in contrast with the zero degree differential cross section, the integrated cross section decreases monotonically above  $\sim 5$  MeV, reflecting the onset of the strong forward peaking. Above  $E_p = 7$  MeV, the total number of  $n_1$  neutrons which leave  ${}^7\text{Be}$  in the first-excited states is always greater than 25% of the number of  $n_0$  neutrons which leave  ${}^7\text{Be}$  in the ground state, reaching a maximum of about 55% at  $E_p \sim 9$  MeV.

A compilation of presently available measured laboratory differential cross sections at zero deg for the  ${}^7\text{Li}(p,n){}^7\text{Be}$   $n_0$  and  $n_1$  (0.0 MeV and 0.43 MeV levels of  ${}^7\text{Be}$ ) reactions and the ratio of  $n_1$  to  $n_0$  neutrons and of measured laboratory integrated cross sections as functions of proton kinetic bombarding energy may be found in our report [5].

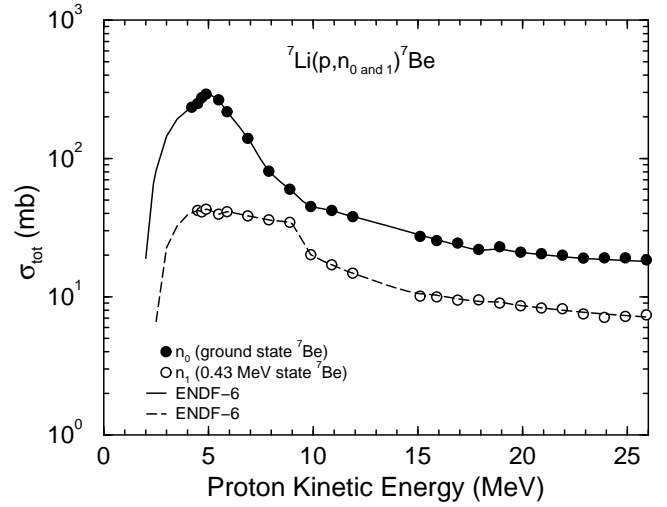


Figure 1: Measured total cross sections for the  ${}^7\text{Li}(p,n_0){}^7\text{Be}$  and  ${}^7\text{Li}(p,n_1){}^7\text{Be}$  reactions between 4 and 26 MeV [12] together with our evaluations in the ENDF-6 [19] format.

### III. EVALUATION METHODS

The production of an evaluated data library for proton reactions on lithium poses certain difficulties. In particular, nuclear model calculations based on statistical preequilibrium and equilibrium decay theories become unreliable for light target nuclei, where the nuclear levels are widely spaced. For this reason, one would like an evaluated data library that is based, as much as possible, on measured data.

We have therefore adopted the following approach. There are numerous measurements of the important  ${}^7\text{Li}(p,n_0)$  and  ${}^7\text{Li}(p,n_1)$  direct reactions populating the ground and first excited states of  ${}^7\text{Be}$ , and we have used these experimental data for the cross sections and

angular distributions in the evaluation. This is important because many aspects of the production of neutron sources via  ${}^7\text{Li}(p,n)$  reactions involve use of the high-energy quasimonoenergetic  $n_0$  and  $n_1$  neutrons. To model the remaining cross section available for nuclear reactions, *i.e.* the overall reaction cross section minus these direct reaction cross sections, we use GNASH nuclear model calculations [20,21].

Use of the GNASH calculations is expected to lead to some weaknesses in the evaluated data, because of the aforementioned difficulties in using a statistical model code. However, we note that the calculations do, at least, include certain important constraints such as energy, flux, angular momentum, and parity, conservation laws. Since the GNASH calculations make use of experimental nuclear levels information, they can also be expected to lead to emission spectra that correctly include peaks and gaps in the calculated energy-dependent spectra at the correct locations, *i.e.* peaks at energies where final states can be excited, and gaps where there are no final nuclear states available.

#### A. Evaluation of $n_0$ and $n_1$ cross sections and angular distributions

The  ${}^7\text{Li}(p,n_0)$  and  ${}^7\text{Li}(p,n_1)$  evaluations were based upon measured data. The center-of-mass measured angular distributions of both the  $n_0$  and  $n_1$  neutrons were fitted using Legendre polynomials,

$$\frac{d\sigma_{c.m.}}{d\Omega} = \sum_{n=0}^N A_n P_n(\cos\theta).$$

For proton incident energies up to 12 MeV, such Legendre fits have been published by Poppe *et al.*, and therefore we adopted their results (Fig. 5 of Ref. [12]).

At higher proton incident energies, we performed Legendre polynomial fits to measured angular distributions. For proton incident energies of 15.1, 15.9, 16.9, 17.9, 18.9, 19.9, 20.9, 22.0, 23.0, 24.0, 25.0, and 26 MeV, there are available measurements separately for  $n_0$  and  $n_1$  by Poppe *et al.* [12]. Above 26 MeV, there are fewer experimental data at only a limited number of incident energies and emission angles, and furthermore, only data for the sum of  $n_0$  and  $n_1$  are available. We used the measurements by Batty *et al.* [22] at 30 and 50 MeV, by Goulding *et al.* [23] at 119.8 MeV, and by Watson *et al.* [24] at 134.2 MeV. We fitted these data using for the ratio  $R = n_1/n_0$  a fixed value of 0.35, as measured by Poppe *et al.* [12] at  $E_p = 25.9\text{MeV}$ , and smoothly interpolated/extrapolated the resulting Legendre coefficients up to  $E_p = 150\text{MeV}$ .

As an example, Fig. 2 shows the sum of  $n_0$  and  $n_1$  measured total production cross section (for references,

see [5]) as a function of proton kinetic energy,  $E_p$ , compared with our evaluation. One can see good agreement in the whole energy range up to 150 MeV.

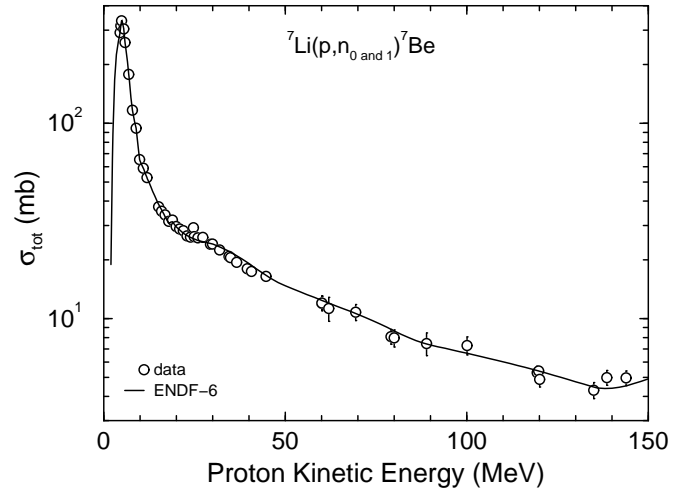


Figure 2: Comparison of the sum of measured [12, 15, 16, 24, and 25] laboratory angle integrated cross sections for the  ${}^7\text{Li}(p,n_0){}^7\text{Be}$  and  ${}^7\text{Li}(p,n_1){}^7\text{Be}$  reactions (for details, see [5]) with our evaluation in the ENDF-6 format.

#### B. GNASH calculations

The latest version of the GNASH code has been described in Ref. [20], and its latest application in nuclear reaction evaluation work has been described in Ref. [4]. For this reason, here we provide only an overview of the models used in the calculations, concentrating on new features.

GNASH calculations of preequilibrium and Hauser-Feshbach decay require input parameter information describing the optical model transmission coefficients, nuclear level densities, gamma-ray strength functions, as well as nuclear level information for all the nuclei that can be populated in the reaction. For most of these quantities, we used default parameter information, as described in Ref. [4]. Below, we provide information on the optical model we used for  ${}^7\text{Li}$ .

Although the appropriateness of an optical potential for nucleon scattering on a light nucleus such as lithium is questionable, we have, for pragmatic reasons, made use of a relativistic potential for  ${}^6\text{Li}$  published by Chiba *et al.* [26]. This potential was shown to provide a surprisingly good representation of available elastic scattering and total cross section data, for energies up to a few hundred MeV [26]. We converted this neutron potential for use on  ${}^7\text{Li}$  by making small isospin corrections, and produced a version for proton scattering

by including Coulomb correction terms. The modified potentials resulted in a calculated total neutron cross section that accounted for measured data fairly well. The calculated proton reaction cross section was also in good agreement with measurements (see Fig. 3).

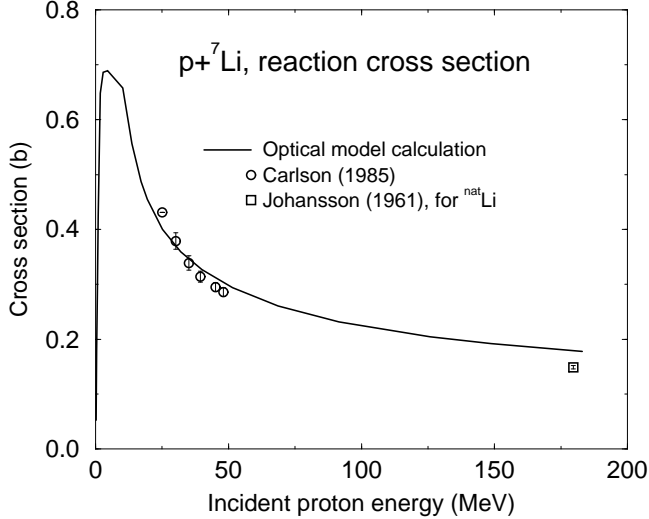


Figure 3: Proton reaction cross section of  ${}^7\text{Li}$ . The solid curve shows values calculated with the optical model by Chiba *et al.* [26] modified here as described in Section III.B. Experimental data are from Refs. [27, 28].

Since the GNASH code includes  $n_0$  and  $n_1$  neutron emission contributions from compound nucleus and preequilibrium decay, these cross sections had to be ignored since, in our evaluation, they are based on measurements. Therefore we wrote a utility code that takes a GNASH output, modifies the  $n_0$  and  $n_1$  neutron emission cross sections to zero, and in the evaluated file introduces the cross sections based on experiment as described in Sec. III A above.

Examples of the  ${}^7\text{Li}(p, xn)$  calculated zero-degree double-differential cross sections of neutrons are shown in Fig. 4, compared with measurements. Solid lines show the results from the GNASH calculations; Dashed-lines show the  $n_0$  and  $n_1$  contributions (evaluated from the measurements). Comparisons are made with  $E_p = 15, 20,$  and  $30$  MeV data of McNaughton *et al.* [13],  $E_p = 40$  MeV data of Jungerman *et al.* [14], and at  $E_p = 55, 90,$  and  $140$  MeV data of Byrd and Sailor [29]. In these figures, in addition to the highest-energy peak due to  $n_0$  and  $n_1$  neutrons, several lower-energy peaks due to  $n_2$  and  $n_3$  neutrons, representing the population of the 4.55- and 6.51-MeV states in  ${}^7\text{Be}$  are evident (see also, e.g., Fig. 2 in Poppe *et al.* [12], where even the peaks by  $n_4$  and  $n_5$ , representing the population of the 7.19- and 10.79-MeV states in  ${}^7\text{Be}$

are clearly observed).

We emphasize that the GNASH results shown in Fig. 4 have not been broadened to account for the experimental detector resolution. This explains why peaks and dips are observed in the calculated energy-dependent spectra, but are not seen so prominently in the experimental data. Overall, it is evident that the evaluation accurately represents the  $n_0$  and  $n_1$  neutrons, as it should since it is based on the experimental data. The lower-energy neutrons from the GNASH calculation agree with the measurements less well, but it is hoped that the accuracy obtained is sufficient for LEDA design calculations.

#### IV. ENDF DATA

In this section we show some graphical representations of the evaluated ENDF data. These figures help illustrate certain features of the evaluation. The figures shown here are a small subset of figures produced automatically by the NJOY code [30]. The full set of figures can be viewed on the T-2 WWW site, by first going to <http://t2.lanl.gov/data/he.html>, registering, and then clicking on premade plots in Postscript format for protons (<http://t2.lanl.gov/data/p-ps/>).

Figure 5 shows the proton elastic scattering angular distribution for incident energies up to 150 MeV. The increased forward-peaking with increasing incident energy is evident. Figure 6 shows the angular distributions, reconstructed from the ENDF Legendre coefficients, for the  $n_0$  and  $n_1$  emitted neutrons.

Four separate figures are combined together in Figure 7. On the top left, the overall cross sections for the  $n_0$ , and  $n_1$  reactions are shown, as is also the “remaining” cross section, designated as MT=5, that is used in the GNASH calculations. The sum of all these cross sections is the reaction cross section as shown in Fig. 3.

In Fig. 7, top right, the inclusive production cross sections are shown for the light ejectiles. Note that, unlike for reactions on heavier nuclei, these do not keep increasing with incident energy up to 150 MeV, but instead become approximately constant above 40 MeV. This energy corresponds, approximately, to the total binding energy of  ${}^7\text{Li}$ , and therefore above this energy it is not possible to obtain additional particle production by increasing the incident energy.

In Fig. 7 lower-left, a perspective plot is shown of the angle-integrated neutron emission spectra obtained from GNASH, as a function of incident energy. The increasing role of preequilibrium high-energy neutron emission is seen as the incident energy increases. Finally, in Fig. 7 lower-right the total heating (MeV/collision) is shown as a function of incident energy. This includes energy transferred to all secondary charged-particles, except protons (since this is the pro-

jectile, and it is therefore assumed that a transport calculation will always be explicitly tracking the secondary protons).

## V. SUMMARY AND FUTURE WORK

Our new evaluation for protons on  ${}^7\text{Li}$  is available in the ENDF-6 format for use in radiation transport calculations. By using and testing these data in simulations of thick and thin lithium targets, we hope to obtain feedback on possible improvements that are needed.

An example of a recent test [3] of our library is shown in Fig. 8. We have modeled the 43-MeV proton source from JAERI's TIARA AVE cyclotron with MCNPX. Protons impinge on a 3.6-mm thick  ${}^7\text{Li}$  target. Resulting neutrons are constrained by an iron collimator 10.9 cm in diameter and 225 cm long. We have modeled this target, assuming a monoenergetic point proton source. The neutron flux is tallied on the surface exiting the collimator. In the report with experimental results [31], the neutron flux is normalized to unity in an energy band between 36.3 and 45.5 MeV. We have normalized our results in the same manner. Two MCNPX calculations were performed, one using tables by our library and the other using the Bertini Intranuclear Cascade Model (INC) in conjunction with a preequilibrium+evaporation model.

Results for the experiment and the two calculations are shown in Fig. 8. Overall, neither calculation is in completely satisfactory agreement with the experiment. This is not surprising given we used a cascade, a preequilibrium, and an evaporation model in the Bertini INC calculations and the physics of the GNASH code for such a light target. However, we observe that the width of the neutron peak more closely matches the experiment when proton tables from our library are used. This could be expected in advance, since we used for the peak a parametrization of experimental data in our tables. The Bertini INC predicts a neutron peak that is lower in energy and much broader than observed.

For completeness, we list here a couple of areas where we know there is room for improvement. The first point emphasizes weaknesses in the ENDF evaluation that may be problematic for simulations above 30 MeV for our case (see details in [5]).

Secondly, our analysis was not developed to include an accurate treatment of gamma-ray production, but instead focussed on neutron emission. Indeed, the nuclear level information in the GNASH calculations describing the decay of excited states by gamma-ray emission was not carefully checked. Therefore, if gamma-ray emission becomes of concern in LEDA target design studies, an upgrade to this evaluation may be needed.

## ACKNOWLEDGMENTS

The authors are grateful to J. L. Ullmann and W. B. Wilson for useful discussions and information.

This study was supported by the U. S. Department of Energy.

## REFERENCES

1. J. C. Browne, J. L. Anderson, M. W. Cappiello, G. P. Lawrence, and P. W. Lisowski, "Status of the Accelerator Production of Tritium (APT) Project," *Proc. APT Symp. The Savannah River Accelerator Project and Complementary Spallation Neutron Sources*, University of South Carolina, Columbia, USA, May 14-15, 1996, p. 14, F. T. Avignone and T. A. Gabriel, Eds., World Scientific, Singapore, (1998).
2. *ED&D Monthly Report, October, 1999*, LA-UR 99-6201, Los Alamos National Laboratory (1999).
3. H. G. Hughes, M. B. Chadwick, R. K. Corzine, H. W. Egdorf, F. X. Gallmeier, R. C. Little, R. E. MacFarlane, S. G. Mashnik, E. J. Pitcher, R. E. Prael, A. J. Sierk, E. C. Snow, L. S. Waters, M. C. White, and P. G. Young, "Status of the MCNPX Transport Code," Los Alamos National Report LA-UR-004942, Proc. Int. Conf. on Advanced Monte Carlo for Radiation Physics, Particle Transport Simulation and Application (MC 2000), 23-26 October, 2000, Lisbon, Portugal.
4. M. B. Chadwick, P. G. Young, S. Chiba, S. Frankle, G. M. Hale, H. G. Hughes, A. J. Koning, R. C. Little, R. E. MacFarlane, R. E. Prael, and L. S. Waters, "Cross Section Evaluation to 150 MeV for Accelerator-Driven System and Implementation in MCNPX," *Nucl. Sci. Eng.*, **131**, 293 (1999).
5. S. G. Mashnik, M. B. Chadwick, P. G. Young, R. E. MacFarlane, and L. S. Waters, " ${}^7\text{Li}(p,n)$  Nuclear Data Library for Incident Proton Energies to 150 MeV," Los Alamos National Laboratory Report LA-UR-00-1067, Los Alamos (2000).
6. M. Drogg, "Sources of Variable Energy Monoenergetic Neutrons for Fusion-Related Applications," *Nucl. Sci. Eng.*, **106**, 279 (1990).
7. J. H. Gibbons and H. W. Newson, "The  ${}^7\text{Li}(p,n){}^7\text{Be}$  Reaction," *Fast Neutron Physics*, Vol. 1, J. B. Marion and J. L. Fowler, Eds., Interscience, New York (1960).
8. J. H. Langsdorf, Jr., J. E. Monahan, and W. A. Reardon, "A Tabulation of Neutron Energies from Monoenergetic Protons on Lithium," ANL-5219, Argonne National Laboratory (Jan. 1954).

9. J. W. Meadows and D. L. Smith, "Neutron Source Investigations in Support of the Cross Section Program at the Argonne Fast-Neutron Generator," ANL/NDM-53, Argonne National Laboratory (May 1980).
10. J. W. Meadows and D. L. Smith, "Neutrons from Proton Bombardment of Natural Lithium," ANL-7938, Argonne National Laboratory (June 1972).
11. J. D. Anderson, C. Wong, and V. A. Madsen, "Charge Exchange Part of the Effective Two-Body Interaction," *Phys. Rev. Lett.*, **24**, 1074 (1970).
12. C. H. Poppe, J. D. Anderson, J. C. Davis, S. M. Grimes, and C. Wong, "Cross Sections for the  ${}^7\text{Li}(p,n){}^7\text{Be}$  Reaction Between 4.2 and 26 MeV," *Phys. Rev. C*, **14**, 438 (1976).
13. M. W. McNaughton, N. S. P. King, F. P. Brady, J. L. Romero, and T. S. Subramanian, "Measurements of  ${}^7\text{Li}(p,n)$  and  ${}^9\text{Be}(p,n)$  Cross Sections at 15, 20, and 30 MeV," *Nucl. Instr. Meth.*, **130**, 555 (1975).
14. J. A. Jungerman, F. P. Brady, W. J. Knox, T. Montgomery, M. R. McGie, J. L. Romero, and Y. Ishizaki, "Production of Medium-Energy Neutrons from Proton Bombardment of Light Elements," *Nucl. Instr. Meth.*, **94**, 421 (1971).
15. S. D. Schery, L. E. Young, R. R. Doering, S. M. Austin, and R. K. Bhowmik, "Activation and Angular Distribution Measurements of  ${}^7\text{Li}(p,n){}^7\text{Be}$  ( $0.0 + 0.429$  MeV) for  $E_p = 25 - 45$  MeV: A Technique for Absolute Neutron Yield Determination," *Nucl. Instr. Meth.*, **147**, 399 (1977).
16. T. E. Ward, C. C. Foster, G. E. Walker, J. Rapaport, and C. A. Goulding, " $1/E$  Dependence of the  ${}^7\text{Li}(p,n){}^7\text{Be}$  (g.s.+0.43 MeV) Total Reaction Cross Section," *Phys. Rev. C*, **25**, 762 (1982).
17. T. N. Taddeucci, W. P. Alford, M. Barlett, R. C. Byrd, T. A. Carey, D. E. Ciskowski, C. C. Foster, C. Gaarde, C. D. Goodman, C. A. Goulding, J. B. McClelland, D. Prout, J. Rapaport, L. J. Rybarczyk, W. C. Sailor, E. Sugaebaker, and C. A. Whitten, Jr., "Zero-Degree Cross Sections for the  ${}^7\text{Li}(p,n){}^7\text{Be}$  (g.s.+0.43 - MeV) Reaction in the Energy Range 80-795 MeV," *Phys. Rev. C*, **41**, 2548 (1990).
18. M. Baba, Y. Nauchi, T. Iwasaki, T. Kiyosumi, M. Yohioka, S. Matsuyama, N. Hirakawa, T. Nakamura, Su. Tanaka, S. Meigo, H. Nakashima, Sh. Tanaka, N. Nakao, "Characterization of 40-90 MeV  ${}^7\text{Li}(p,n)$  Neutron Source at TIARA Using a Proton Recoil Telescope and a TOF Method," *Nucl. Instr. Meth. A*, **428**, 454 (1999).
19. V. McLane, "ENDF-102 Data Formats and Procedures for the Evaluated Nuclear Data File ENDF-6," BNL-NCS-44945, Rev. 2/97, Brookhaven National Laboratory, National Nuclear Data Center (1997).
20. P. G. Young, E. D. Arthur, and M. B. Chadwick, "Comprehensive Nuclear Model Calculations: Theory and Use of the GNASH Code," *Proc. IAEA Workshop on Nuclear Reaction Data and Nuclear Reactors — Physics, Design, and Safety*, Trieste, Italy, April 15 - May 17, 1996, p. 227, A. Gandini and G. Reffo, Eds., World Scientific Publishing, Ltd., Singapore (1998).
21. P. G. Young, E. D. Arthur, and M. B. Chadwick, "Comprehensive Nuclear Model Calculations: Introduction to the Theory and Use of the GNASH Code," LA-12343-MS, Los Alamos National Laboratory (1992).
22. C. J. Batty, B. E. Bonner, A. I. Kilvington, C. Tschalär, and L. E. Williams, "Intermediate Energy Neutron Sources," *Nucl. Instrum. Methods*, **68**, 273 (1969).
23. C. A. Goulding, M. B. Greenfield, C. C. Foster, T. E. Ward, J. Rapaport, D. E. Bainum, and C. D. Goodman, "Comparison of the  ${}^{12}\text{C}(p,n){}^{12}\text{N}$  and  ${}^{12}\text{C}(p,p')$  Reactions at  $E_p = 62$  and  $120$  MeV," *Nucl. Phys. A*, **331** 29 (1979).
24. J. W. Watson, R. Pourang, R. Abegg, W. P. Alford, A. Celler, S. El-Kateb, D. Frekers, O. Häusser, R. Helmer, R. Henderson, K. Hicks, K. P. Jackson R. G. Jeppesen, C. A. Miller, M. Vetterli, S. Yen, and C. D. Zafratos, " ${}^7\text{Li}(p,n){}^7\text{Be}$  and  ${}^{12}\text{C}(p,n){}^{12}\text{N}$  Reactions at 200, 300, and 400 MeV," *Phys. Rev. C*, **40**, 22 (1989).
25. J. W. Watson, B. D. Anderson, A. R. Baldwin, C. Lebo, B. Flanders, W. Pairsuwan, R. Madey, and C. C. Foster, "A Comparison of Methods for Determining Neutron Detector Efficiencies at Medium Energies," *Nucl. Instrum. Methods*, **215**, 413 (1983).
26. S. Chiba, K. Togasaki, M. Ibaraki, M. Baba, S. Matsuyama, N. Hirakawa, K. Shibata, O. Iwamoto, A. J. Koning, G. M. Hale, and M. B. Chadwick, "Measurements and Theoretical Analysis of Neutron Elastic Scattering and Inelastic Reactions Leading to a Three-Body Final State for  ${}^6\text{Li}$  at 10 to 20 MeV," *Phys. Rev. C*, **58**, 2205 (1998).
27. R. F. Carlson, A. J. Cox, T. N. Nasr, M. S. De Jong, D. L. Ginther, D. K. Hasell, A. M. Sourkes, W. T. H. Van Oers, and D. J. Margaziotis, "Measurements of Proton Total Reaction Cross Sections for  ${}^6\text{Li}$ ,  ${}^7\text{Li}$ ,  ${}^{14}\text{N}$ ,  ${}^{20}\text{Ne}$ , and  ${}^{40}\text{Ar}$  Between 23 and 49 MeV," *Nucl. Phys. A*, **445**, 57 (1985).

28. A. Johansson, U. Svanberg, and O. Sundberg, "Total Nuclear Reaction Cross Sections for 180 MeV Protons," *Arkin für Physik*, **19**, 527 (1961).
29. R. C. Byrd and W. C. Sailor, "Neutron Detection Efficiency for NE213 and BC501 Scintillators at Energies Between 25 and 200 MeV," *Nucl. Instrum. Methods A*, **274**, 494 (1989).
30. R. E. MacFarlane, "Recent Progress on NJOY," LA-UR-96-4688, Los Alamos National Laboratory (1996); the last version of the code, NJOY99, is described on the Web page at <http://t2.lanl.gov/codes/codes.html>.
31. N. Nakao, H. Nakashima, T. Nakamura, S. Tanaka, S. Tanaka, K. Shin, M. Baba, Y. Sakamoto, and Y. Nakane, "Transmutation Through Shields of Quasi-Monoenergetic Neutrons Generated by 43-MeV and 68-MeV Protons – I: Concrete Shielding Experiment and Calculation for Practical Application," *Nucl. Sci. Eng.*, **124**, 228 (1996).

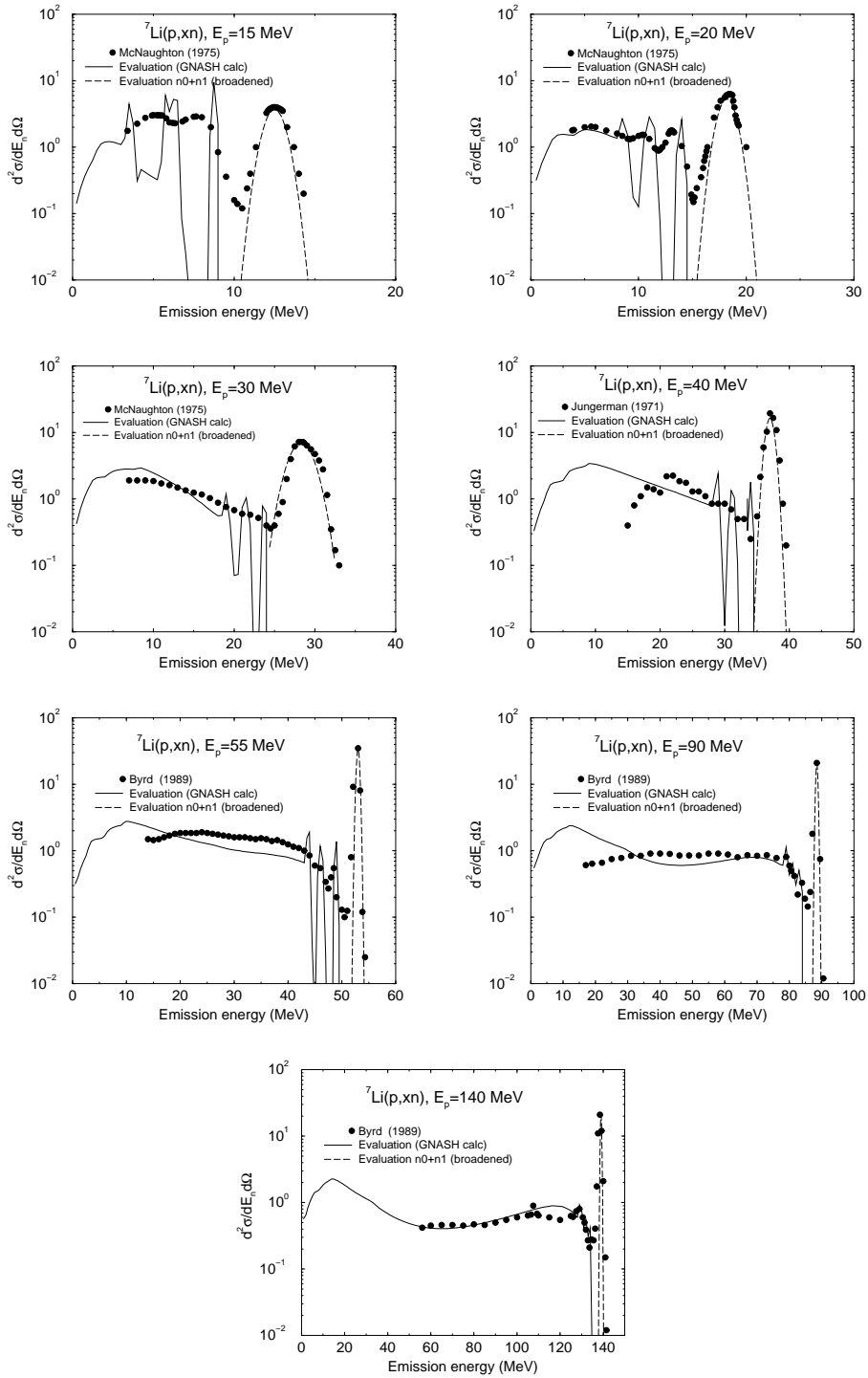


Figure 4: Zero degree neutron emission from the  ${}^7\text{Li}(p,xn)$  reaction. Solid lines show the results from the GNASH calculations, dashed lined show  $n_0$  and  $n_1$  contributions evaluated from the measurements. The GNASH-calculated spectra have not been broadened using the experimental resolution. Data are from Refs. [13, 14, 29].



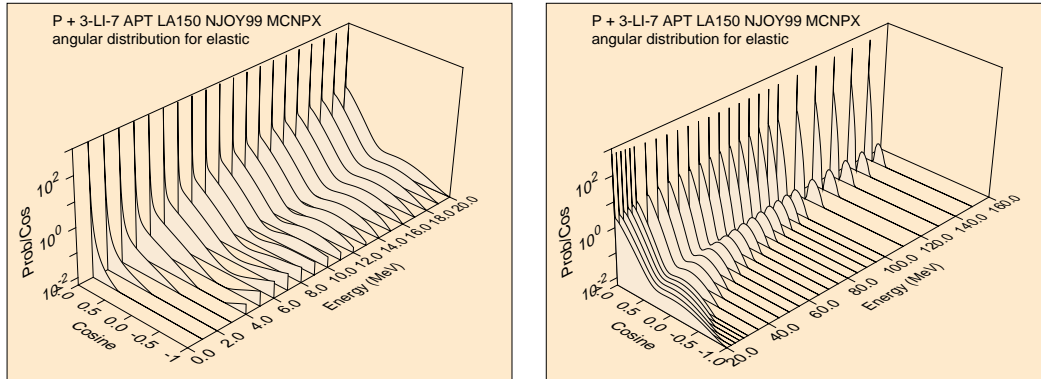


Figure 5: Proton elastic scattering angular distribution of  ${}^7\text{Li}$  at different incident energies up to 150 MeV.

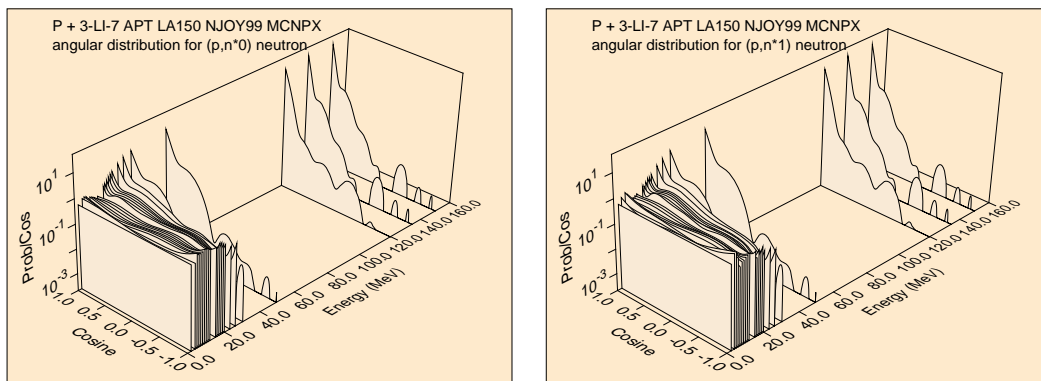


Figure 6: Angular distributions for  $n_0$  and  $n_1$  neutrons from  $p + {}^7\text{Li}$  interactions at different incident energies up to 150 MeV.

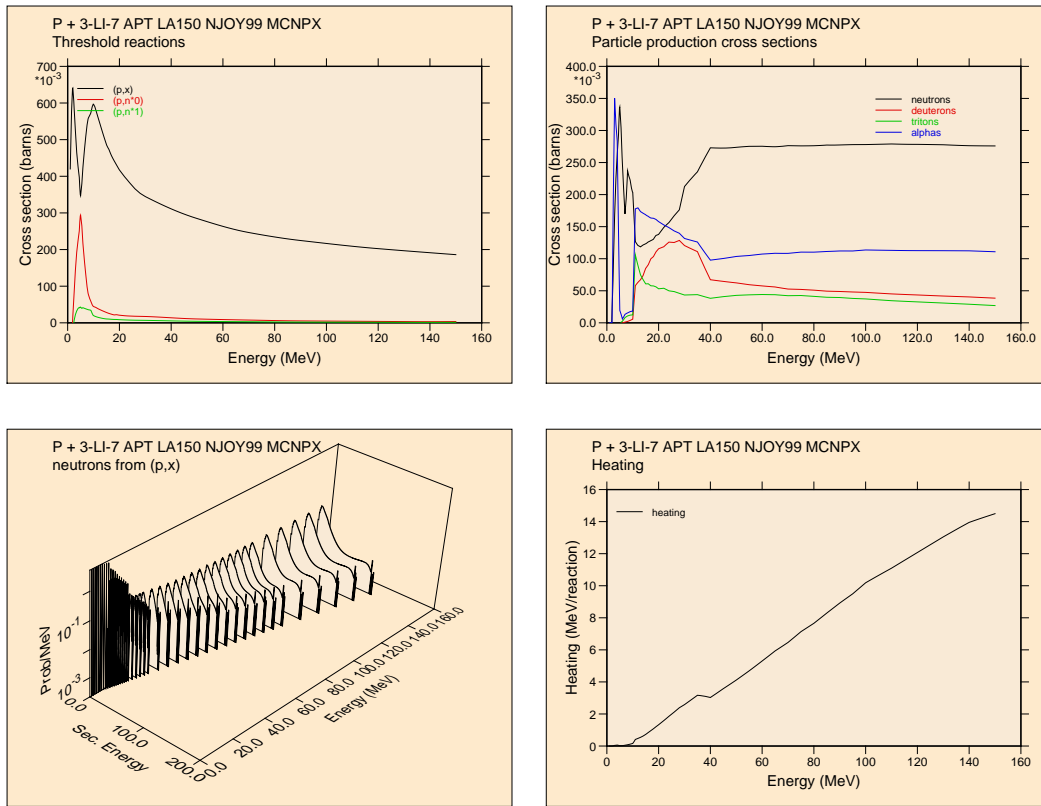


Figure 7: Different channel cross sections, neutron angle-integrated energy spectra, and heating (MeV/collision) as functions of incident energy for  $p + {}^7\text{Li}$  interactions, as indicated.

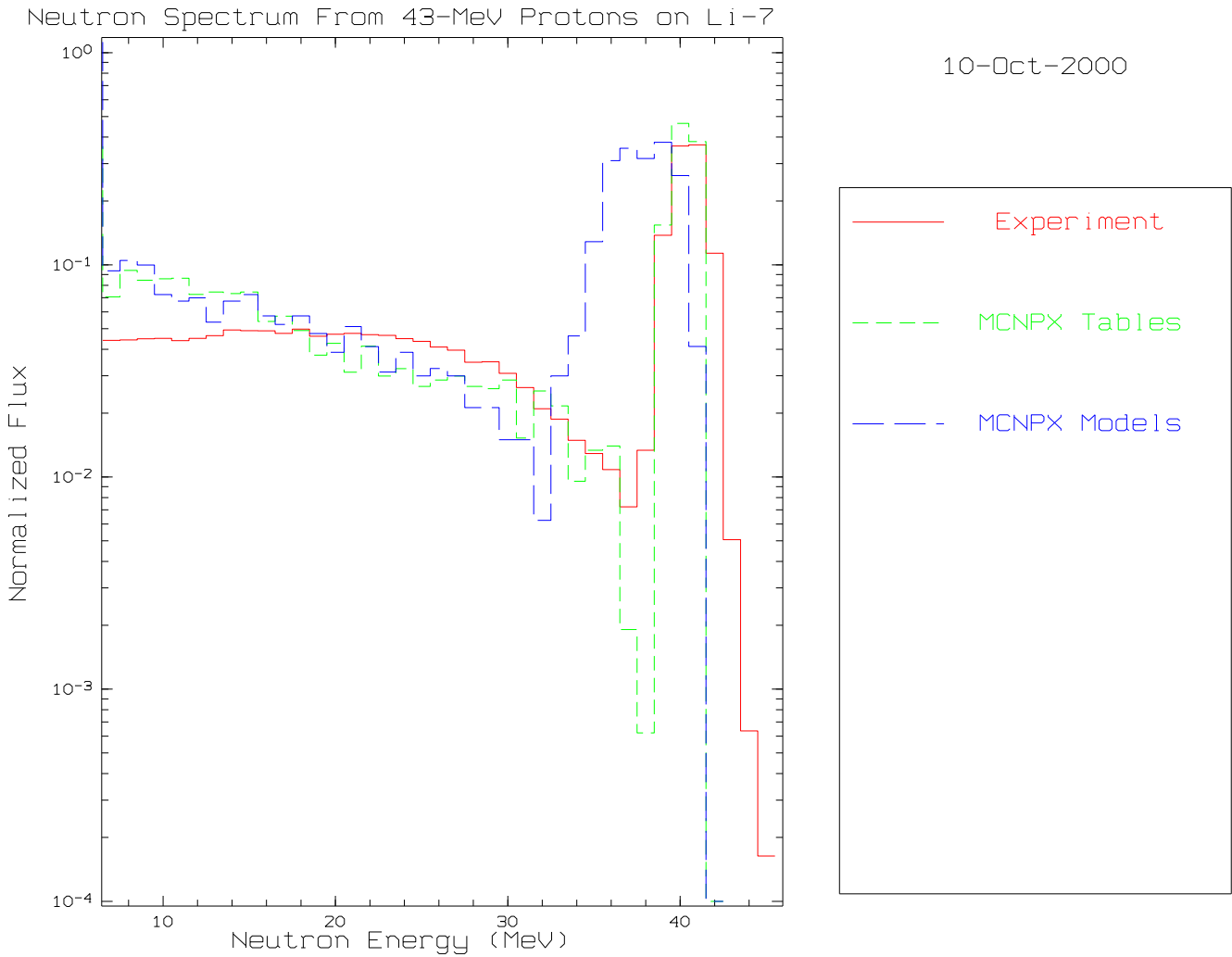


Figure 8: Neutron flux from a 3.6-mm thick  ${}^7\text{Li}$  target normalized to unity in the energy band between 36.3 and 45.5 MeV calculated with MCNPX using our data library (dashed histogram) and results by the Bertini INC in conjunction with a preequilibrium+evaporation model (long-dashed histogram) compared with the experimental data from [31] (solid histogram).